Electronic Supplementary Material (ESI) for Physical Chemistry Chemical Physics.

Supporting Information

Multi-band perfect absorber based on elliptical cavity coupled elliptical metal nanorod structure

Yizhao Pan[1], Yuchang Li[1], Fang Chen [1]*, Shubo Cheng[1], Wenxing Yang[1], Boyun Wang[2], Zao Yi[3]

**Correspondence: Fang Chen (chenfang@yangtzeu.edu.cn)*

[1]Institute of Quantum Optics and Information Photonics, School of Physics and Optoelectronic Engineering, Yangtze University, Jingzhou 434023, People's Republic of China

[2]School of Physics and Electronics-informantion Engineering, Hubei Engineering University, Xiaogan 432000, China

[3]Joint Laboratory for Extreme Conditions Matter Properties, Southwest University of Science and Technology, Mianyang 621010, China

Section 1. The absorption property of triple-band absorber under the TE polarization.

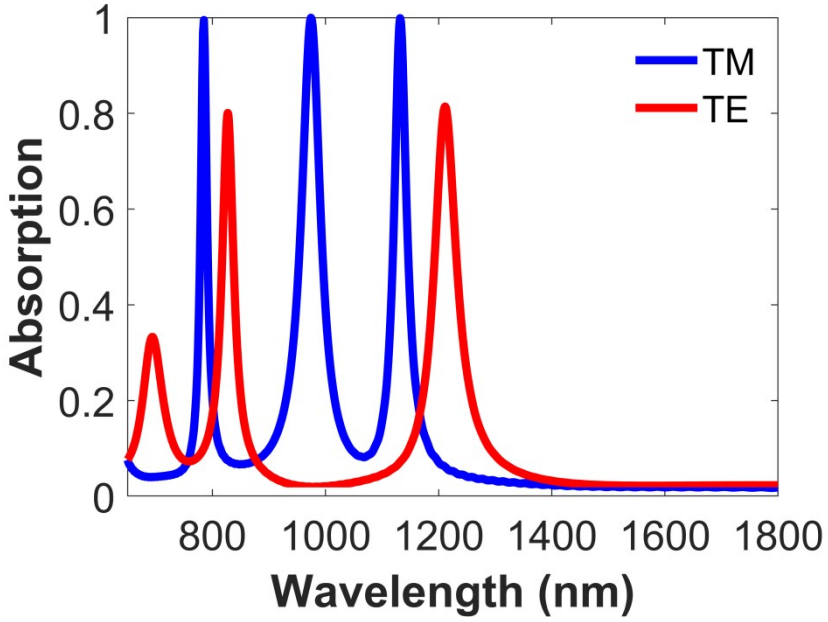

Fig. S1. The absorption spectra of the triple-band under the TM and TE polarization.

Fig.S1 shows the absorption spectra of the triple-band absorber under the TM and TE polarization. The incident angle is zero, only two significant absorption peaks located at 835 nm and 1236 nm can be observed. The comparison chart of the CMT fitted spectrum and the FDTD simulation spectrum is exhibited in Fig. S2. The curve still fits very well. To study the physical mechanism of the two absorption peaks, the electric field distributions are presented in Fig. S3. For 835 nm, a strong electric field is distributed at the upper and lower inner edges of the elliptic cavity (called transverse mode) [1], the design of an elliptical cavity provides more degrees of freedom to excite modes in different directions. The larger long half-axis leads to a larger transverse mode wavelength of excitation. But unlike TM polarized light excitation, the local surface plasmon polaritons resonance of the silver elliptical pillar cannot be excited. Due to the turning of the electric field, as shown in Fig.S3 (e) and (f), there is no energy localized in the dielectric layer between the elliptical silver pillar and the lower silver layer, resulting in an absorption peak of only about 80%.

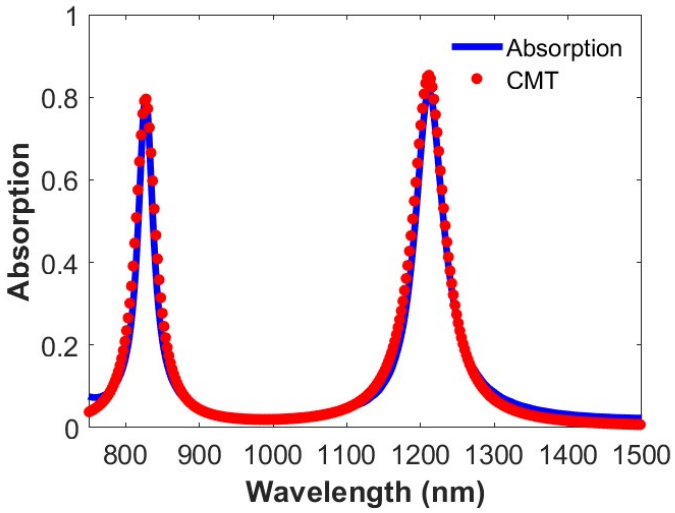

Fig. S2. The FDTD spectrum and the CMT spectrum under TE polarization.

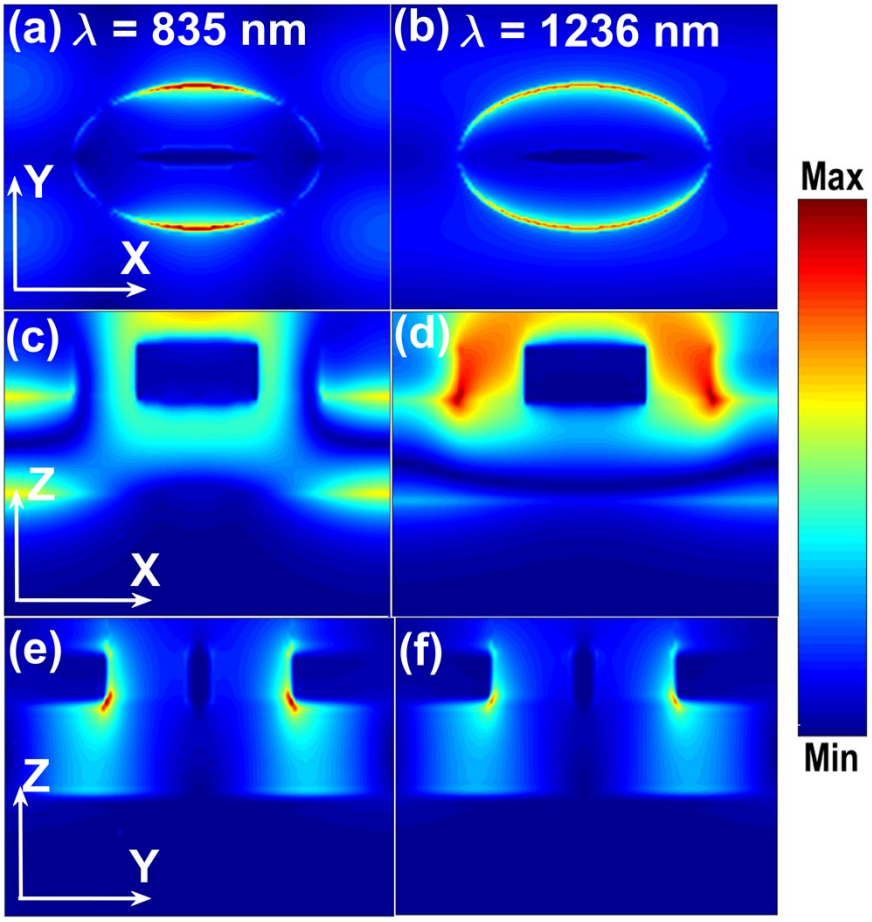

Fig. S3. The field distribution of the two resonant modes. (a)-(b): electric-field distributions in the x-y plane; (c)-(d): electric-field distributions in the x-z plane; (e)-(f): electric-field distributions in the y-z plane at different wavelengths.

Section 2. The absorption property of the four-band absorber under the TE polarization.

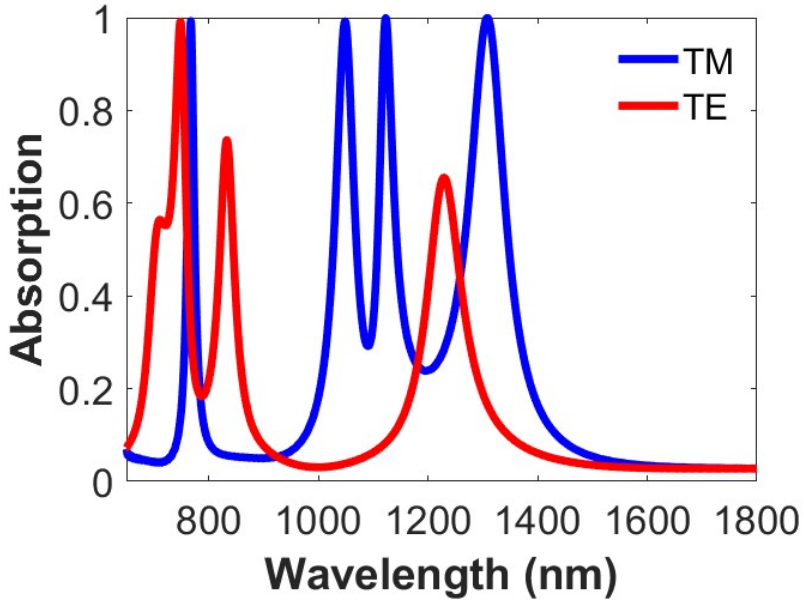

Fig. S4. The absorption spectra of the four-band under the TM and TE polarization.

Fig.S4 shows the absorption spectra of the four-band absorber under the TM and TE polarization. The incident angle is zero, and three significant absorption peaks located at 748 nm, 833 nm, and 1229 nm can be observed. The comparison chart of the CMT fitted spectrum and the FDTD simulation spectrum is exhibited in Fig. S5. To study the physical mechanism of the three absorption peaks, the electric field distributions are shown in Fig. S6. For 748 nm, the longitudinal localized plasmon resonance mode supported by the two larger ellipsoid pillars is excited [2]. We can notice the gap between the elliptical pillars is only 15 nm, a strong field is compressed in the gap, resulting in an enhanced absorption of 100%. For 833 nm, the transverse mode is excited at the upper and lower inner edges of the elliptic cavity, partial electric field is located in the gap between ellipsoid pillars. Similarly, for 1229 nm, we can see the same phenomenon. As shown in Fig.S6 (h) and (i), there is no energy localized in the dielectric layer between the elliptical silver pillar and the lower silver layer, a partial energy distributed in the dielectric layer between the elliptical air cavity and the lower silver layer. Ultimately, the absorption rates of the two peaks are 73.65%, and 65.51%, respectively.

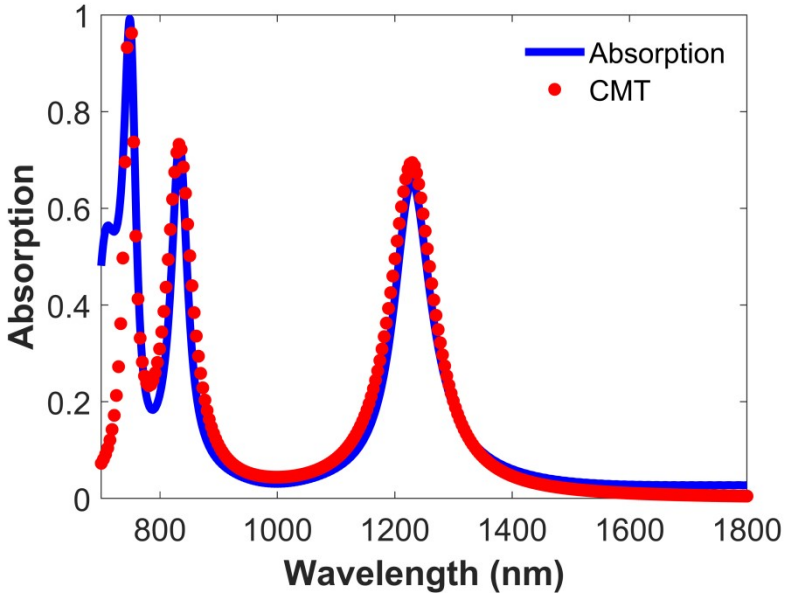

Fig. S5. The FDTD spectrum and the CMT spectrum.

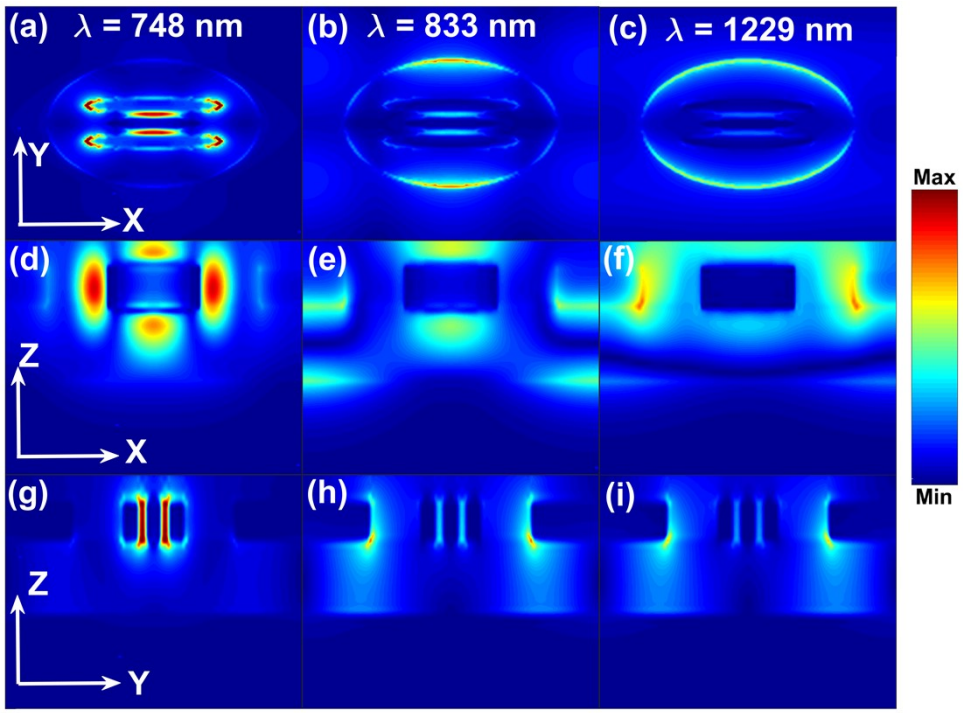

Fig. S6. The field distribution of the three resonant modes. (a)-(c): electric-field distributions in the x-y plane; (d)-(f): electric-field distributions in the x-z plane; (g)-(i): electric-field distributions in the y-z plane at different wavelengths.

Section 3. The absorption spectra with different dispersion models.

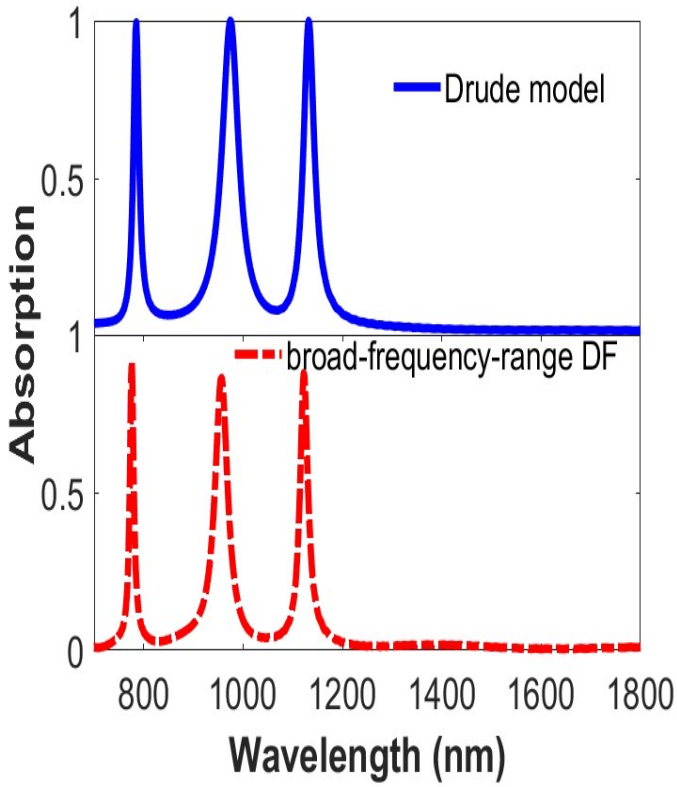

Fig. S7. The absorption spectra with the Drude model and the broad-frequency-range dielectric constant model.

Fig. S7 shows the absorption spectra with the Drude model and the broad-frequency-range dielectric constant model. The dielectric constant of silver can be expressed by [3]:

$$\varepsilon_{drude}(\omega)=\varepsilon_{real}(\omega)+\varepsilon_{imag}(\omega)=\varepsilon_{\infty}-\frac{\omega_p^2}{\omega(\omega+i\gamma_c)}$$

$$\varepsilon_m(\omega)=\varepsilon_{free}(\omega)+\varepsilon_{ib}(\omega)$$

$$\varepsilon_{free}(\omega)=1-\frac{\omega_p^2}{\omega(\omega+i\gamma_c)}$$

$$\varepsilon_{ib}(\omega)=Re(\varepsilon_{ib}(\omega))+Im(\varepsilon_{ib}(\omega))$$

$$Im(\varepsilon_{ib}(\mathrm{h}\omega))=\varepsilon_{lo}+\frac{\varepsilon_{up}-\varepsilon_{lo}}{1+e^{S\cdot\mathrm{h}(\omega_c-\omega)}}$$

$$Re(\varepsilon_{ib}(\mathrm{h}\omega))=\frac{A}{\mathrm{h}^2(\omega-\omega_c)^2+(\mathrm{h}\gamma_L)^2}$$

ε_m	External	Interband Contribution			Fitted		Free Electron Contribution	
	$\hbar\omega_c[eV]$	ε_{ip}	ε_{lo}	$S[1/eV]$	$A[eV^2]$	$(\hbar\gamma_L)^2[eV^2]$	$\omega_p[eV]$	$\gamma[eV]$
Ag	3.9	6.37–0.54 [1/eV]·$\hbar\omega$	0.1	7.9	4.02	1.00	9.0	0.020

Table S1. The parameters for the broad-frequency-range model of silver

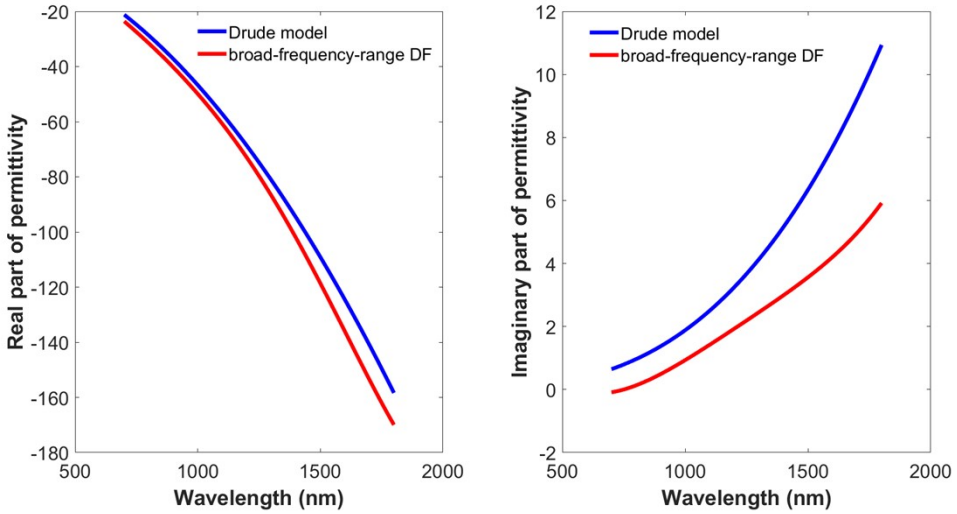

Fig. S8. The real and imaginary parts of the dielectric constant calculated by the Drude model and broad-frequency-range model

As is known to all, the absorption of electromagnetic wave by silver takes place by intraband and interband transitions which occur in different wavelength ranges. Intraband transitions contribute to the infrared absorption of free electrons as in the Drude model, while interband transitions contribute to the vacuum ultraviolet absorption of free electrons as in the broad-frequency-range model. The advantage of using the Drude model is its simplicity, and its results are reasonable when the wavelength of light is bigger than 308 nm (3.2 eV). You can see that the positions of absorption peaks are almost identical from Fig. S7, but the absorption efficiency is lower when calculated by the broad-frequency-range model. This is because the imaginary part of the dielectric constant is lower when using the broad-frequency-range model, which can be seen in Fig.S8.

Reference:

1.Kolwas, K. (2023). Optimization of Coherent Dynamics of Localized Surface Plasmons in Gold and Silver Nanospheres; Large Size Effects. *Materials*, 16(5), 1801.

2.Malola, S., Lehtovaara, L., Enkovaara, J., & Hakkinen, H. (2013). Birth of the localized surface plasmon resonance in monolayer-protected gold nanoclusters. *Acs Nano*, 7(11), 10263-10270.

3.Kolwas, K., & Derkachova, A. (2020). Impact of the interband transitions in gold and silver on the dynamics of propagating and localized surface plasmons. *Nanomaterials*, 10(7), 1411.